Radio Science, Volume 29, Number 4, Pages 799–814, July–August 1994

Polarimetric passive remote sensing of ocean wind vectors

S. H. Yueh, R. Kwok, F. K. Li, S. V. Nghiem, and W. J. Wilson
Jet Propulsion Laboratory, California Institute of Technology, Pasadena

J. A. Kong
Research Laboratory of Electronics, Massachusetts Institute of Technology, Cambridge

Abstract. This paper investigates the theory of polarimetric passive remote sensing of wind-generated sea surfaces and the potential application of polarimetric radiometry to ocean wind remote sensing. Theoretical polarimetric emission coefficients of small-scale sea surfaces are evaluated using the small perturbation method (SPM). The SPM is derived to second order and applied to the Stokes vectors of thermal emission from random rough dielectric surfaces described by anisotropic directional spectra. To verify the accuracy of the SPM, a Monte Carlo simulation is performed to calculate the Stokes vectors of the emission from the simulated one-dimensional random rough surfaces with a power law spectrum for various observation angles and surface parameters. The theoretical results of the SPM for all four Stokes parameters are in excellent agreement with the numerical results obtained from the Monte Carlo simulation. Moreover, the second-order coherent fields are indispensable in the theoretical evaluation of the third and fourth Stokes parameters. Otherwise, the reflectivities of random rough surfaces would be significantly overestimated, and the signs of the third and fourth Stokes parameters would be incorrect. The SPM is then applied to small-scale sea surfaces described by an empirical sea surface spectrum. It is found that the azimuthal signatures of Stokes parameters agree qualitatively well with aircraft Ku-band radiometer data. Theoretical model functions of the Stokes parameters are illustrated. Advantages of wind direction retrieval using polarimetric Q and U measurements are discussed, and it is expected that a spaceborne polarimetric radiometer has a potential of providing wind vector measurements with uniform accuracy across all parts of swath.

1. Introduction

There has been an increasing interest in the microwave passive polarimetry of geophysical media [*Tsang*, 1991]. Theoretical calculations for the Stokes parameters of the thermal emission have been presented for one-dimensional periodic dielectric surfaces [*Veysoglu et al.*, 1991] and for one-dimensional oceanlike rough surfaces with a prescribed power law spectrum [*Yueh and Kwok*, 1992; *Johnson et al.*, 1994]. The theoretical predictions were verified by the measured Stokes parameters of thermal emission from periodic soil surfaces at X band [*Nghiem et al.*, 1991] and measurements over water surfaces impressed with a fiberglass layer with a sinusoidal profile at *Ku* band [*Yueh et al.*, 1994] and at X band [*Johnson et al.*, 1994]. All the results show that the Stokes parameters are functions of the azimuth angle between the observation direction and the corrugation direction of surfaces. However, further analysis and experiments are necessary for two-dimensional rough surfaces.

Recently, it has been shown by *Etkin et al.* [1991] and *Wentz* [1992] that the brightness temperatures of horizontal and vertical polarizations T_h and T_v of ocean surfaces vary as functions of the azimuth angles. Etkin et al. found the dependence of brightness temperatures on the azimuth angle during circle flights using their aircraft radiometers at nadir viewing with frequencies of 3.75, 20, and 37.5 GHz and a 20-GHz radiometer for grazing angle ($\theta = 78°$) observations. It was observed that the directional dependence rapidly dropped with decreasing electromagnetic frequencies. However, the measurements were not made for the middle range of incidence angles, which is important for space remote sensing when spatial coverage and resolution

Paper number 94RS00450.
0048-6604/94/94RS-00450$08.00

need to be considered together. In the results published by *Wentz* [1992], the data investigated were collected by the special sensor microwave/imager (SSM/I), which cannot measure the third Stokes parameter. After being coregistered with the buoy-measured wind vector, T_h and T_v at both 19 and 37 GHz were found to be dependent on wind direction. The results indicate that the directional feature of water surfaces contributes to the azimuthal variation of brightness temperatures.

Besides the observations for T_h and T_v reported above, *Dzura et al.* [1992] presented the first experimental evidence of the azimuthal variations of polarimetric brightness temperatures of sea surfaces, though the measurements were made at normal incidence, and only one case was presented. Figure 5 in their paper showed that when the second Stokes parameter (Figure 5b) reached maximum, the third Stokes parameter (Figure 5c) was nearly zero, and vice versa. No explanation was provided in their paper for this observed signatures, whereas in this paper we show that for nadir observations, the second and third Stokes parameters should behave like cos 2ϕ and sin 2ϕ, respectively, which will explain the reported azimuthal signatures. However, since only one example was reported and since the results were collected at nadir observation angles, more extensive experiments and analyses of the azimuthal variations of the Stokes parameters over wind speeds and incidence angles are required to evaluate the applicability of polarimetric radiometry to ocean surface winds.

In view of the recent observations, a theoretical analysis based on the small perturbation method (SPM) is presented in this paper to extend the theoretical calculations to two-dimensional random rough surfaces to evaluate the contribution to polarimetric emissivities from the small-scale sea surfaces (capillary waves), which are the source of the Bragg scattering at microwaves. The SPM has been used previously to derive the sea surface emission at microwaves by *Wu and Fung* [1972] for isotropic random rough surfaces. However, their theory predicted no azimuthal dependence of brightness temperatures because the surface spectrum was assumed to be isotropic. Furthermore, the third and fourth Stokes parameters are expected to be zero from their theory, unlike the results presented in this paper where we generalize the theory to random surfaces with anisotropic wavenumber spectra. Additionally, the accuracy of the SPM for surface emission is evaluated with results obtained from a Monte Carlo simulation technique for one-dimensional rough surfaces. This comparison has not been presented in the literature to the authors' knowledge, though quite a lot of work has been done in verifying the SPM for ocean surface scattering in active remote sensing.

In section 2, the theory of polarimetric radiometry is summarized, and a polarimetric version of Kirchhoff's law is presented to relate the Stokes vector to the polarimetric bistatic scattering coefficients. Section 3 summarizes the results of the SPM derived to second order for rough surfaces with anisotropic directional spectra. Section 4 compares the results of the SPM with the Monte Carlo simulation technique for the polarimetric emission from one-dimensional random rough surfaces characterized by a power law spectrum. Section 5 applies the SPM to the Stokes vectors of thermal emission from the small-scale wind-generated sea surfaces described by an empirical wavenumber spectrum and compares the theoretical results with aircraft radiometer measurements made by *Dzura et al.* [1992]. Section 6 discusses advantages of polarimetric radiometry for ocean wind vector retrieval. Section 7 summarizes the results of this paper and discusses other important issues regarding the application of polarimetric radiometry for ocean wind vector retrieval.

2. Polarimetric Radiometry

For microwave polarimetric radiometry, thermal emission is described by a Stokes vector I_s with four parameters, T_h, T_v, U, and V,

$$I_s = \begin{bmatrix} T_h \\ T_v \\ U \\ V \end{bmatrix} = c' \begin{bmatrix} \langle E_h E_h^* \rangle \\ \langle E_v E_v^* \rangle \\ 2\ \mathrm{Re}\ \langle E_v E_h^* \rangle \\ 2\ \mathrm{Im}\ \langle E_v E_h^* \rangle \end{bmatrix}, \tag{1a}$$

where T_h and T_v are the brightness temperatures of horizontal and vertical polarizations, and U and V characterize the correlation between these two polarizations. The second equality defines the Stokes parameters in terms of the horizontally and vertically polarized components of electric fields (E_h and E_v) illustrated in Figure 1. The definitions of the h pol, v pol, and wave vectors are the same as those used by *Yueh et al.* [1988]. The angular brackets denote the ensemble average of the argument, and

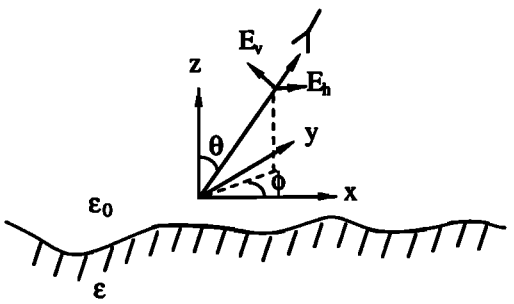

Figure 1. Configuration.

c' is a proportional constant [*Yueh and Kwok*, 1993].

Besides the above definition, an alternative definition of the Stokes vector has also been widely used in remote sensing [*Tsang et al.*, 1985]:

$$I_s' = \begin{bmatrix} I \\ Q \\ U \\ V \end{bmatrix} = \begin{bmatrix} T_v + T_h \\ T_v - T_h \\ U \\ V \end{bmatrix}. \tag{1b}$$

Both definitions contain exactly the same information. However, as to be shown later in this section, this definition will render a convenient representation in illustrating the emission from small-scale sea surfaces at near-nadir observation angles.

For the development of geophysical model functions, which relate the thermal radiation signatures to the geophysical surface parameters, the Stokes parameters are usually expressed in the Fourier series of the azimuth angle ϕ. For wind-generated sea surfaces it is expected that the surfaces are statistically reflection symmetric with respect to the wind direction represented by $\phi = 0$. (We will assume that there are no strong swell components that are not aligned with the wind.) Because of the reflection symmetry, it can be shown that I and Q are even functions of ϕ, whereas U and V are odd functions. Hence to the second harmonics of ϕ,

$$\begin{aligned} I &\simeq I_0 + I_1 \cos\phi + I_2 \cos 2\phi \\ Q &\simeq Q_0 + Q_1 \cos\phi + Q_2 \cos 2\phi \\ U &\simeq U_1 \sin\phi + U_2 \sin 2\phi \\ V &\simeq V_1 \sin\phi + V_2 \sin 2\phi. \end{aligned} \tag{2}$$

When there is no up/downwind asymmetry in the surface features (e.g., untilted small-scale sea surfaces), the spectral density of the surface is symmetric with respect to the origin, and the Stokes vector can be shown to consist of the following symmetry

$$I_s(\phi) = I_s(\phi + \pi), \tag{3}$$

which implies that $I_1 = Q_1 = U_1 = V_1 = 0$. Hence the Fourier series can be further simplified to

$$\begin{aligned} I &\simeq I_0 + I_2 \cos 2\phi \\ Q &\simeq Q_0 + Q_2 \cos 2\phi \\ U &\simeq U_2 \sin 2\phi \\ V &\simeq V_2 \sin 2\phi. \end{aligned} \tag{4}$$

Note that the relations defined in (4) are derived purely based on the symmetry assumption and are valid for any incidence angle θ as long as the surface features do not have up/downwind asymmetry.

Azimuth Dependence at Nadir Viewing

A special case that is worth noting is the azimuth dependence of Stokes parameters at normal incidence or nadir viewing, which can be derived by using a coordinate rotation transformation. This case would provide a simple explanation of the azimuth modulations in Q and U measurements made by *Dzura et al.* [1992].

Let us assume that the vertical polarization channel of an antenna positioned at $\phi = 0$ is parallel to the wind direction, and when the antenna is positioned at an angle ϕ or observes the surface from an azimuth angle ϕ, its vertical polarization channel makes an angle of ϕ and $\pi/2 - \phi$, respectively, with the vertical and horizontal polarization channels of the antenna at $\phi = 0$. Therefore the horizontally and vertically polarized electric fields measured by the antenna positioned at any azimuth angle ϕ are related to those (E_{h0} and E_{v0}) measured at $\phi = 0$ by the rotation transformation:

$$\begin{aligned} E_v(\phi) &= E_{v0} \cos\phi + E_{h0} \sin\phi \\ E_h(\phi) &= -E_{v0} \sin\phi + E_{h0} \cos\phi. \end{aligned} \tag{5}$$

Using the above equation together with the definition of Stokes parameters, it easily can be shown that the Stokes parameters measured at any azi-

muth angle ϕ are related to the brightness temperatures of horizontal and vertical polarizations (T_{h0} and T_{v0}) measured at $\phi = 0$.

$$\begin{aligned} I(\phi) &= T_{v0} + T_{h0} \\ Q(\phi) &= (T_{v0} - T_{h0}) \cos 2\phi \\ U(\phi) &= -(T_{v0} - T_{h0}) \sin 2\phi \\ V(\phi) &= 0, \end{aligned} \tag{6}$$

where the fact that both U and V are zeros at $\phi = 0$ have been used in the derivation.

The above relations derived at normal incidence show that the Stokes parameters Q and U have a $\cos 2\phi$ and a $\sin 2\phi$ variations, respectively, and I is not a function of ϕ. In addition, (4) confirms the form of model function shown in (16) inferred from theoretical data.

Polarimetric Kirchhoff's Law

In the following, we discuss how the emissivity of rough surfaces can be related to the bistatic scattering coefficients of the surfaces by the Kirchhoff's law, which was originally derived by *Peake* [1959] for any polarization for surfaces with a uniform temperature. By a straightforward extension of Peake's argument [*Yueh and Kwok*, 1993], the Stokes vector of the thermal emission from the surface plus all the reflected downwelling unpolarized radiation is unpolarized and has the same specific intensity as the downwelling radiation, when the surface is in thermal equilibrium with the surroundings. Consequently, the Stokes vector of the thermal emission from the surface with the surface temperature T_s is,

$$I_s = I_z - I_r, \tag{7}$$

where I_z is the Stokes vector for an unpolarized radiation

$$I_z = T_s \begin{bmatrix} 1 \\ 1 \\ 0 \\ 0 \end{bmatrix} \tag{8}$$

and I_r corresponds to the total radiation reflected by the surfaces from the downwelling radiation. In terms of the polarimetric bistatic scattering coefficients $\gamma_{\alpha\beta\mu\nu}$ (see Appendix 1) integrated over all the incident angles in the upper hemisphere, I_r can be expressed as

$$I_r = \int_0^{\pi/2} \sin\theta_i \, d\theta_i \int_0^{2\pi} d\phi_i \frac{\cos\theta_i}{4\pi \cos\theta} \cdot \begin{bmatrix} \gamma_{hhhh}(\theta, \phi; \theta_i, \phi_i) + \gamma_{hvhv}(\theta, \phi; \theta_i, \phi_i) \\ \gamma_{vvvv}(\theta, \phi; \theta_i, \phi_i) + \gamma_{vhvh}(\theta, \phi; \theta_i, \phi_i) \\ 2\,Re\,(\gamma_{vhhh}(\theta, \phi; \theta_i, \phi_i) + \gamma_{vvhv}(\theta, \phi; \theta_i, \phi_i)) \\ 2\,Im\,(\gamma_{vhhh}(\theta, \phi; \theta_i, \phi_i) + \gamma_{vvhv}(\theta, \phi; \theta_i, \phi_i)) \end{bmatrix} \tag{9}$$

Here θ and ϕ signify the zenith and azimuth angles of the observation direction.

3. SPM for Anisotropic Random Rough Surfaces

This section presents the expression of the Stokes vector derived using the second-order SPM for surfaces with anisotropic directional spectra. The surface scattering problem is formulated by the extended boundary condition method, which relates the surface tangential fields to the incident fields. Subsequently, the equations for the surface fields are solved to second order by the perturbation method for small rms height. Here we summarize the results and refer readers to the paper by *Yueh et al.* [1988] for the detailed SPM formulation and derivation.

As the SPM is applied to random rough surfaces, the scattered field can be decomposed into coherent and incoherent components. The zero-order scattered field is a coherent field propagating in the specular reflection direction without depolarization, and its amplitude is characterized by the Fresnel reflection coefficients $R_{hh}^{(0)}$ and $R_{vv}^{(0)}$ for horizontal and vertical polarizations, respectively. However, the first-order scattered field is incoherent and contributes to the lowest-order incoherent bistatic scattering coefficients. As the SPM is derived to second order for surfaces with anisotropic directional spectra, we find that the second-order scattered field is coherent and gives a correction to the coherent reflection coefficients of the surfaces. Furthermore, the cross-polarized components of the second-order coherent field are not zero when the incident direction is not aligned with the symmetry directions of surfaces.

In conclusion, the modified coherent reflection

matrix with the zero- and second-order fields considered can be written as

$$R = \begin{bmatrix} R_{hh} & R_{hv} \\ R_{vh} & R_{vv} \end{bmatrix} = \begin{bmatrix} R_{hh}^{(0)} + R_{hh}^{(2)} & R_{hv}^{(2)} \\ R_{vh}^{(2)} & R_{vv}^{(0)} + R_{vv}^{(2)} \end{bmatrix}, \tag{10}$$

where $R_{\alpha\beta}^{(2)}$ is the reflection coefficient of the α-polarized component of the second-order scattered field with β-polarized, unit amplitude incidence and is related to the spectral density function $W(k_x, k_y)$ by the following integral:

$$R_{\alpha\beta}^{(2)} = \int_{-\infty}^{\infty} \int_{-\infty}^{\infty} dk_x\, dk_y W(k_{xi} - k_x, k_{yi} - k_y) f_{\alpha\beta}^{(2)}, \tag{11}$$

where k_{xi} and k_{yi} are the transverse components of the incident wave vector, and the expression of $f_{\alpha\beta}^{(2)}$ is given in Appendix 3.

Additionally, the incoherent polarimetric bistatic scattering coefficients due to the first-order scattered field can be expressed as

$$\gamma_{\alpha\beta\mu\nu}^{i}(\theta, \phi; \theta_i, \phi_i) = \frac{4\pi k_0^2 \cos^2\theta \Gamma_{\alpha\beta\mu\nu}(k_x, k_y, k_{xi}, k_{yi}) W(k_x - k_{xi}, k_y - k_{yi})}{\cos\theta_i}, \tag{12}$$

where k_0 is the free space wavenumber, and θ_i and ϕ_i correspond to the zenith and azimuth angles of the incidence direction, respectively. Likewise, θ and ϕ represent the zenith and azimuth angles of the scattering direction, respectively. The expressions of $\Gamma_{\alpha\beta\mu\nu}$, k_x, k_y, k_{xi}, and k_{yi} are given in Appendix 2.

Given the above results, I_r can be decomposed into I_{rc} and I_{ri}, the coherent and incoherent surface reflectivities, respectively. That is,

$$I_r = I_{rc} + I_{ri}, \tag{13}$$

where I_{ri} is obtained from (9) by replacing $\gamma_{\alpha\beta\mu\nu}$ with $\gamma_{\alpha\beta\mu\nu}^{i}$, and the coherent reflectivity vector I_{rc} can be written as

$$I_{rc} = \begin{bmatrix} |R_{hh}|^2 + |R_{hv}|^2 \\ |R_{vv}|^2 + |R_{vh}|^2 \\ 2\,Re\,(R_{vh}R_{hh}^* + R_{vv}R_{hv}^*) \\ 2\,Im\,(R_{vh}R_{hh}^* + R_{vv}R_{hv}^*) \end{bmatrix}$$

$$- \begin{bmatrix} |R_{hh}^{(2)}|^2 + |R_{hv}^{(2)}|^2 \\ |R_{vv}^{(2)}|^2 + |R_{vh}^{(2)}|^2 \\ 2\,Re\,(R_{vh}^{(2)}R_{hh}^{(2)*} + R_{vv}^{(2)}R_{hv}^{(2)*}) \\ 2\,Im\,(R_{vh}^{(2)}R_{hh}^{(2)*} + R_{vv}^{(2)}R_{hv}^{(2)*}) \end{bmatrix}. \tag{14}$$

Note that $R_{\alpha\beta}^{(2)}$ and $\gamma_{\alpha\beta\mu\nu}^{i}$ are of the same order because both of them are proportional to the spectral density W. Hence we remove the square of $R_{\alpha\beta}^{(2)}$ in order to have the terms included only up to the same order of magnitude.

4. Comparison of the SPM With the Monte Carlo Simulation

In order to verify the accuracy of the Stokes vector derived using the second-order SPM for anisotropic random rough surfaces, we carry out a Monte Carlo simulation for the polarimetric emissivities of one-dimensional random rough surfaces with a power law spectrum. In simulating the rough surfaces, the surface spectral density function is assumed as follows:

$$W(k_x, k_y) = q \sum_{n=1}^{10} k_x^{-3} \delta(k_x - nk_l)\delta(k_y), \tag{15}$$

where δ is the delta function, and $k_l = 2\pi/5\lambda$ is the low-wavenumber cutoff. Here λ is the electromagnetic wavelength. Independent random numbers with the Gaussian distribution are generated for the real and imaginary parts of each Fourier component of the surfaces and further weighted by the desired spectral density $k_x^{-3/2}$. The simulated Fourier spectra are then transformed to the spatial domain by the fast Fourier transform. Each simulated surface is five wavelengths long and has 40 samples per wavelength. The surface height between these sampled points is linearly interpolated to create a continuous surface profile. Ten surfaces are generated, and the factor q is adjusted for the desired rms surface height (σ). The surfaces simulated by this approach are periodic with the period corresponding to the low-wavenumber cutoff. To solve the scattering coefficients of all the reflected Floquet modes for both horizontally and vertically polarized incident waves, the method of moments with triangular basis for surface tangential fields and pulse weighting is used. Once the scattering coefficients

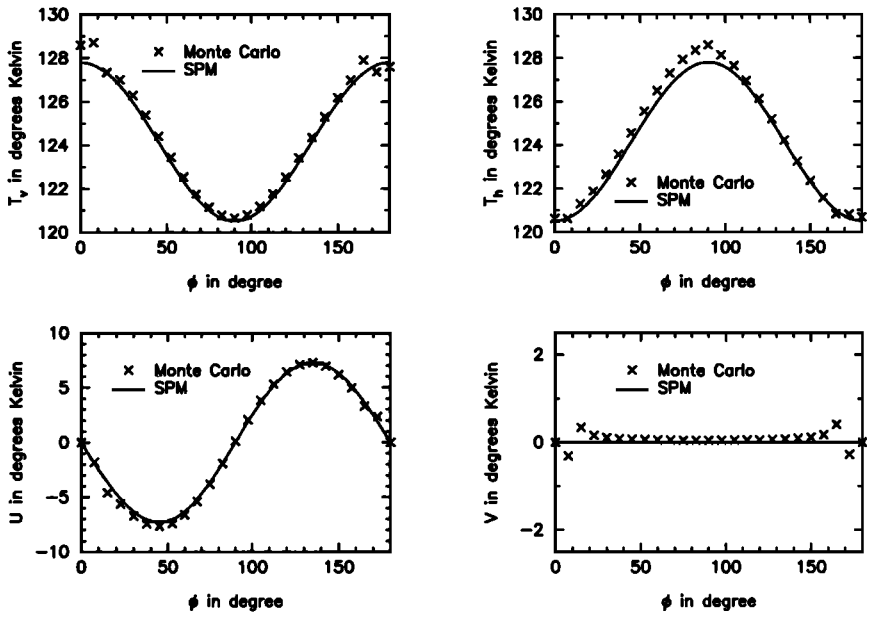

Figure 2. Comparison of polarimetric Stokes vectors versus the azimuth angle ϕ calculated by using Monte Carlo simulation and the SPM for one-dimensional periodic random rough surfaces with $\sigma = \lambda/15$ (or $k_0\sigma = 0.419$) for $\theta = 0$. The permittivity of the surfaces is $45 + i30$, and T_s is 300° Kelvin.

are obtained, the Stokes vectors of the thermal emission from the simulated random surfaces are calculated using Kirchhoff's law. Finally, the average of the Stokes vectors of these ten realizations is taken to represent the Stokes vector of the random surfaces.

Figure 2 illustrates the Stokes parameters as a function of the azimuth angle ϕ for nadir viewing ($\theta = 0°$). The rms surface height is $\lambda/15$, which can be translated into $k_0\sigma = 0.419$. The dielectric constant of $45 + i30$ is assumed for the surfaces. The results calculated using the SPM are in close agreement with those obtained from the Monte Carlo simulation. Additionally, it is found that the Stokes parameters have a cos 2ϕ variation in azimuth for T_h and T_v, sin 2ϕ for U, and zero for V, which are expected for nadir viewing according to (6).

Figure 3 presents the results for off-nadir viewing with $\theta = 50°$, while other parameters are the same as those used for Figure 2. Again, excellent agreement is seen between the SPM and the Monte Carlo simulation. Note that in Figure 3 the Stokes parameters have sharp transitions across many particular azimuth angles. Those are caused by the transition of a particular Floquet mode from radiation to evanescence or vice versa at these angles, which is a special feature of periodic surface scattering [*Yueh et al.*, 1988].

In Figure 4 we plot the Stokes parameters as functions of the zenith angle θ with a fixed azimuth angle of $\phi = 45°$. The SPM and the Monte Carlo simulation agree very well with each other. For most zenith angles, the third Stokes parameter U is about $-2°$ Kelvin, and the fourth Stokes parameter V remains much smaller than U.

Next, we raise the rms surface height by 1.5 times to $\lambda/10$, and the results are presented in Figures 5 and 6 for a fixed θ or ϕ, respectively. The signatures observed are essentially the same as those seen in Figures 3 and 4, except that the magnitudes of variation increase by a factor of 2.25 or a square of 1.5 as expected because the correction terms of the coherent reflection coefficients ($R^{(2)}_{\alpha\beta}$) and the incoherent bistatic scattering coefficients ($\gamma^i_{\alpha\beta\mu\nu}$) are both proportional to the square of rms surface height.

To demonstrate the significance of the corrections introduced by the second-order coherent field, we illustrate the components of the reflectivity vectors I_r, I_{rc}, and I_{ri} in Figures 7 and 8 for the results presented in Figures 3 and 4. Note that the magnitudes of incoherent and coherent components

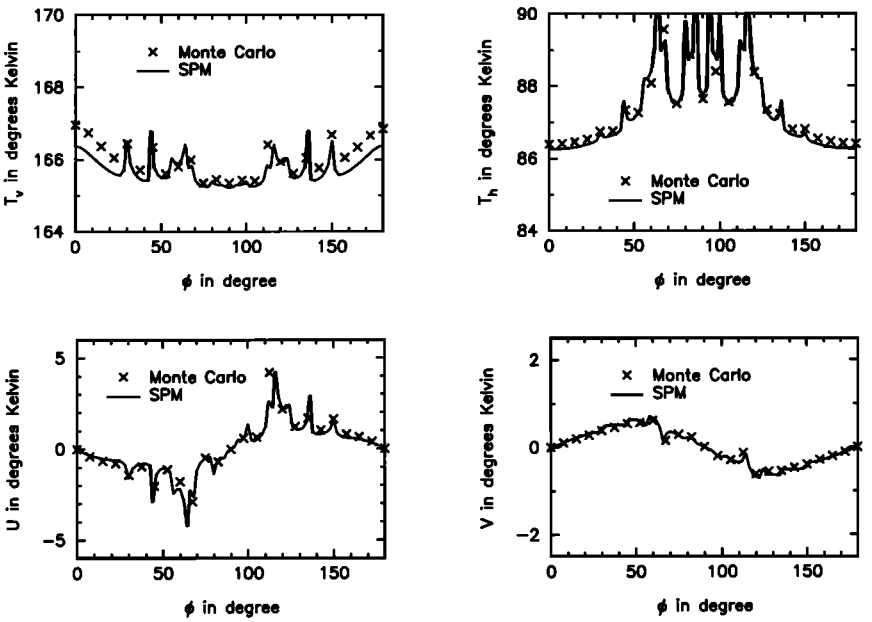

Figure 3. Same as Figure 2 except for $\theta = 50°$.

of U always increase or decrease together, while carrying a different sign. In particular, the total U is always smaller than either one of them. This shows that it is necessary to include the corrections due to the second-order coherent field in the calculation of the Stokes vector. Otherwise, significant errors are expected in the magnitude and the signs of the third Stokes parameter.

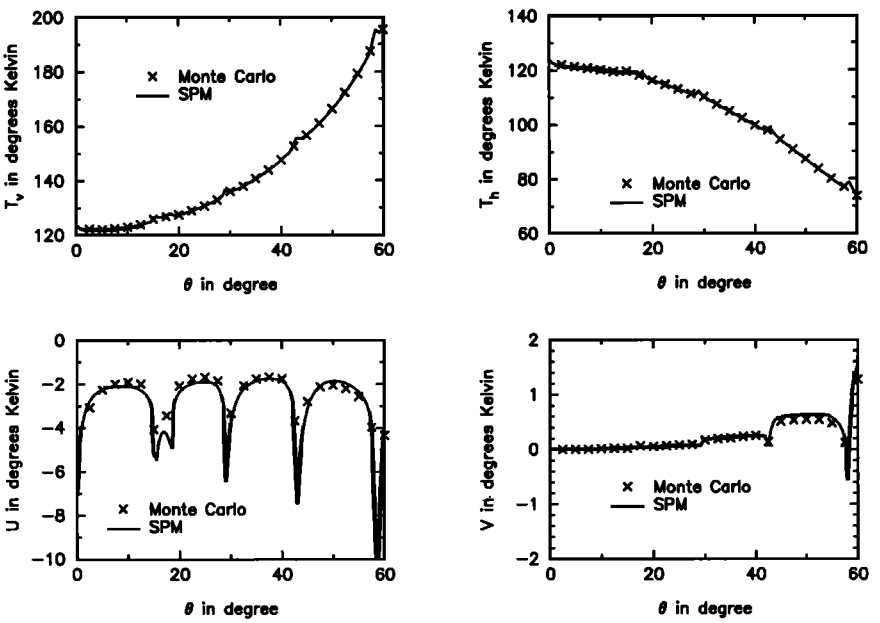

Figure 4. Comparison of polarimetric Stokes vectors versus the θ calculated by using Monte Carlo simulation and the SPM for one-dimensional periodic random rough surfaces with $\sigma = \lambda/15$ (or $k_0\sigma = 0.419$) for $\phi = 45°$. The permittivity of the surfaces is $45 + i30$, and T_s is 300° Kelvin.

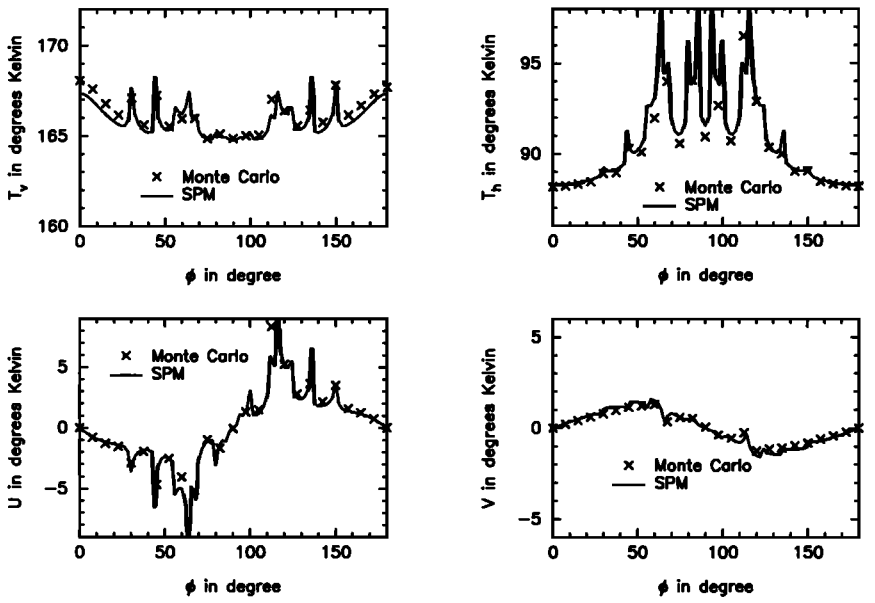

Figure 5. Same as Figure 2 except for $\sigma = \lambda/10$ (or $k_0\sigma = 0.628$).

5. Emission From Small-Scale Sea Surfaces

This section applies the SPM to untilted small-scale sea surfaces and studies the form of geophysical model functions for polarimetric brightness temperatures. Here we do not consider the tilting effects of large-scale surface variations and other sea surface features, such as foams or whitecaps, which are known to be important microwave emission sources [*Smith*, 1988]. Nevertheless, we compare the theoretical polarimetric signatures with the data reported by *Dzura et al.* [1992] to study the effects of small-scale surfaces.

The small-scale wind-induced surfaces are described by an empirical sea surface spectrum pro-

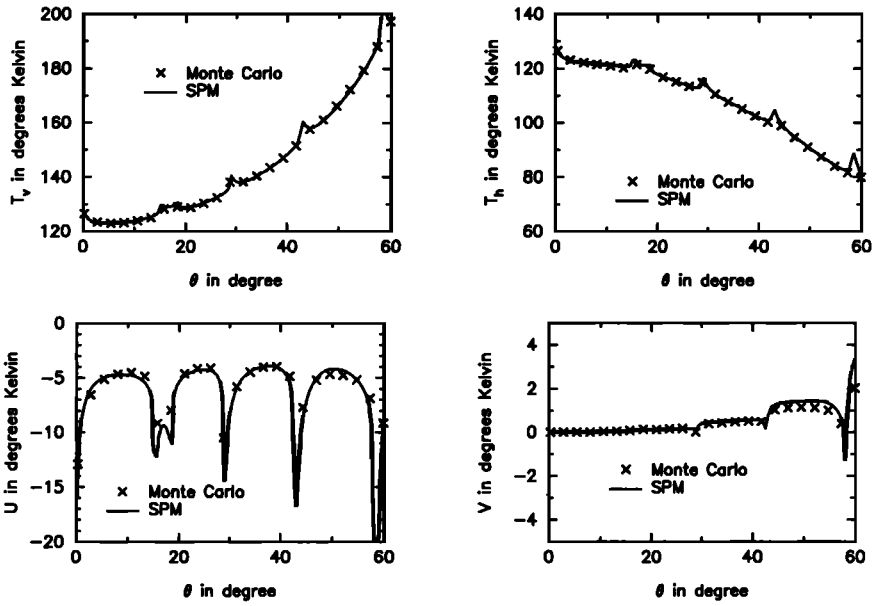

Figure 6. Same as Figure 2 except for $\sigma = \lambda/10$ (or $k_0\sigma = 0.628$).

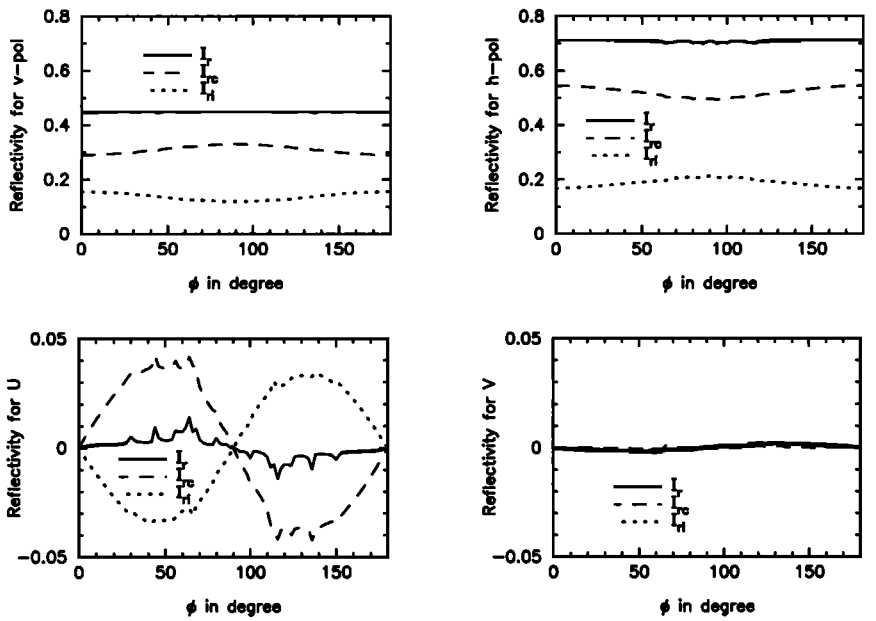

Figure 7. Coherent and incoherent reflectivities of one-dimensional rough surfaces calculated by using the SPM for $\theta = 50°$. Parameters are the same as those used for Figure 2.

posed by *Durden and Vesecky* [1985]. (On account of some typographical errors found in their paper, the correct expressions of spectrum-related formulas are included in Appendix 4.) The choice of this spectrum, instead of many other forms of sea spectrum, for investigating sea surface emissions is because the theoretical backscattering coefficients calculated using this spectrum function were shown

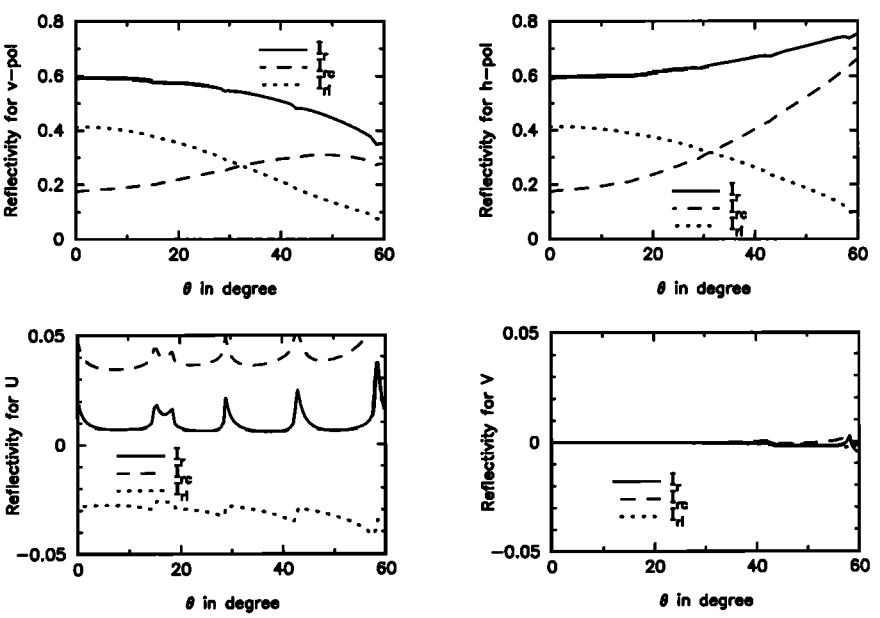

Figure 8. Coherent and incoherent reflectivities of one-dimensional rough surfaces calculated by using the SPM for $\phi = 45°$. Parameters are the same as those used for Figure 2.

Table 1. Small-Scale Sea Surface Roughness Parameter $k_0\sigma$ Versus Wind Speeds for the Cutoff Wavenumbers $k_d = 60$ and 80 at $f = 14$ GHz

$U_{19.5}$, m/s	$k_0\sigma$, $k_d = 60$	$k_0\sigma$, $k_d = 80$
5	0.21	0.16
10	0.29	0.23
15	0.36	0.29
20	0.42	0.34

The parameter σ is the rms height of small-scale surface.

to agree reasonably well with many aircraft measurements by Durden and Vesecky. This implies that Durden and Vesecky's spectrum should be a reasonably good model of sea surfaces, though its absolute accuracy remains to be investigated.

In this paper we let the spectrum of small-scale surfaces be the same as that of the complete spectrum for the wavenumbers above a certain cutoff k_d and be zero otherwise. Table 1 shows the roughness parameter $k_0\sigma$ for two wavenumber cutoffs ($k_d = 60$ and 80) at 14 GHz (*Ku* band) for four wind speeds with the spectral parameter $a_0 = 0.006$, which is 1.5 times that used by *Durden and Vesecky* [1985]. Note that the values of $k_0\sigma$ for these cases are all less than 0.42. Hence we should expect the SPM to be applicable to these cases according to the results presented in the previous section.

Figure 9 compares the aircraft radiometer measurements [*Dzura et al.*, 1992] with the theoretical results plotted as functions of the azimuth angle for nadir viewing at $f = 14$ GHz with $k_d = 80$. Theoretical calculations with $k_d = 60$ have also been carried out, and the results are very close to those with $k_d = 80$. The measurement data were read from Figure 5 of *Dzura et al.* [1992] and represent the average through the curves at each azimuth angle with an expected uncertainty of ±0.5°. It can be seen that the directional features of theoretical Stokes parameters Q and U are just like those of one-dimensional surfaces presented in the previous section, and the magnitudes of azimuthal variations increase as the wind speed increases. In addition, the directional dependence of Stokes parameters Q and U agree fairly well with the aircraft radiometer measurements, though the theoretical results for 10 m/s wind speed, which was the wind speed estimated by Dzura et al., slightly underpredict the magnitude of azimuthal variations. This discrepancy could be caused by the difference between the assumed and true sea surface spectra or the sea surface features (such as, tilting effects of large-scale surfaces and foams) which are not considered in this paper.

To investigate the effects of the spectrum magnitude a_0, we present in Figure 10 the theoretical azimuthal brightness signatures for 10 m/s wind speed for three values of a_0. As expected, when the value of a_0 increases, the magnitudes of brightness variations increase. In addition, it is shown that the theoretical results for $a_0 = 0.008$ agrees very well with the measurements. However, it should be noticed that the spectrum magnitude of 0.008 is two times the value assumed by *Durden and Vesecky* [1985]. This difference in spectral magnitude could

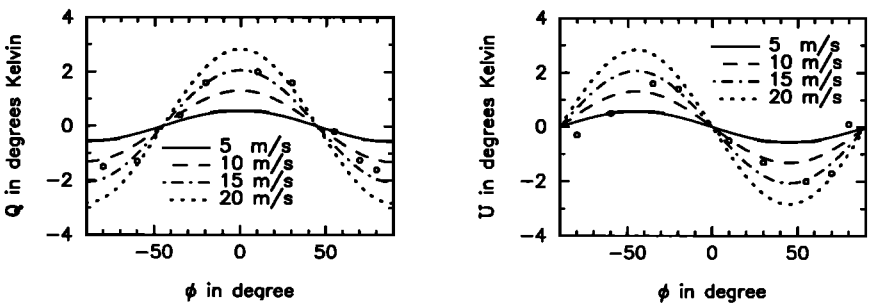

Figure 9. Comparison of the theoretical azimuth dependence of the Stokes parameters with experimental data at nadir viewing. The wavenumber cutoff k_d is 80, $f = 14$ GHz, and $T_s = 10°$ Celsius. Salinity is 35‰. Permittivity of sea surface is calculated by using the empirical formula presented by *Klein and Swift* [1977]. Experimental data, indicated by circles, represent the average through the curves in Figure 5 of *Dzura et al.* [1992] at each azimuth angle with a typical uncertainty of ±0.5 degree.

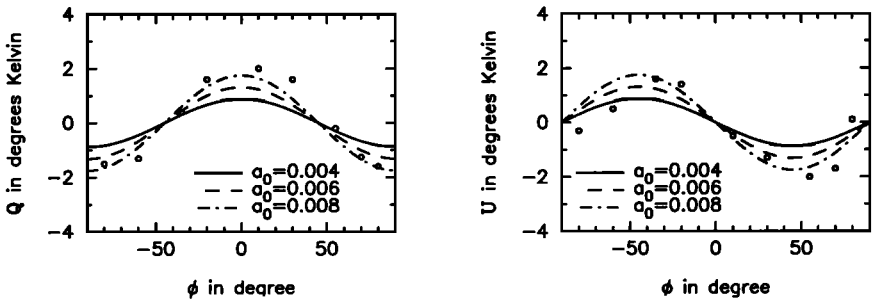

Figure 10. Theoretical sensitivity on the spectrum amplitude a_0 for 10 m/s wind speed. The parameters are the same as those assumed in Figure 9. Experimental data are indicated by circles.

in fact account for the tilting effects of large-scale surface variations and other sea surface features such as foams and breaking waves. Further investigations on the effects of these features are required. Nevertheless, the agreement between the results of the SPM and the measurements indicate that the anisotropic directional features of small-scale wind-generated water ripples play a significant role in the azimuthal signatures of brightness temperatures.

In Figures 11 and 12 we illustrate the Fourier expansion coefficients of Stokes parameters as functions of wind speeds at various zenith angles at $f = 19.3$ GHz with the surface parameters the same as those used for Figure 9. The roughness parameters for $k_d = 100$ and $k_d = 120$ are shown in Table 2. Figure 11a shows that for all zenith angles, I_0 is a monotonically increasing function of wind speed. However, as shown in Figure 11b, Q_0 is fairly insensitive to the wind speed at near-nadir viewing. This suggests that the Stokes parameter I is a better indicator of the wind speed than the parameter Q.

Figure 12 illustrates the coefficients of the second harmonics as functions of wind speeds. As expected, the magnitudes of Q_2 and U_2 increase as the wind speed increases, because of the increase in surface roughness at higher wind speeds. Furthermore, I_2 is zero at $\theta = 0°$ and deviates from zero as θ increases, indicating that the parameter I is insensitive to the wind direction at near-nadir angles. Another interesting feature is that Q_2 is approximately equal to the negative of U_2 for θ smaller than 40°. This relation has been shown to be exact for $\theta = 0°$ in section 2 and explains the azimuthal signatures illustrated in Figure 5 of *Dzura et al.* [1992].

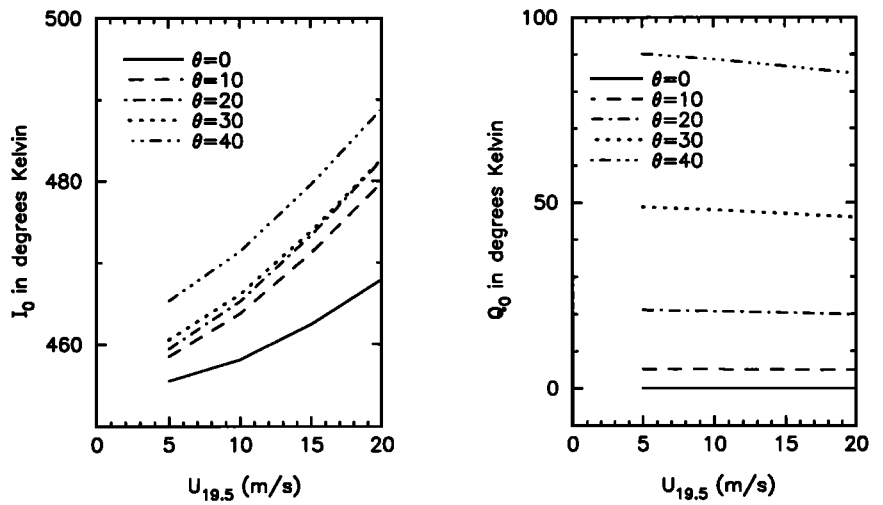

Figure 11. Wind speed dependence at 19.35 GHz. Surface parameters are the same as those of Figure 9. The cutoff wavenumber k_d is 120.

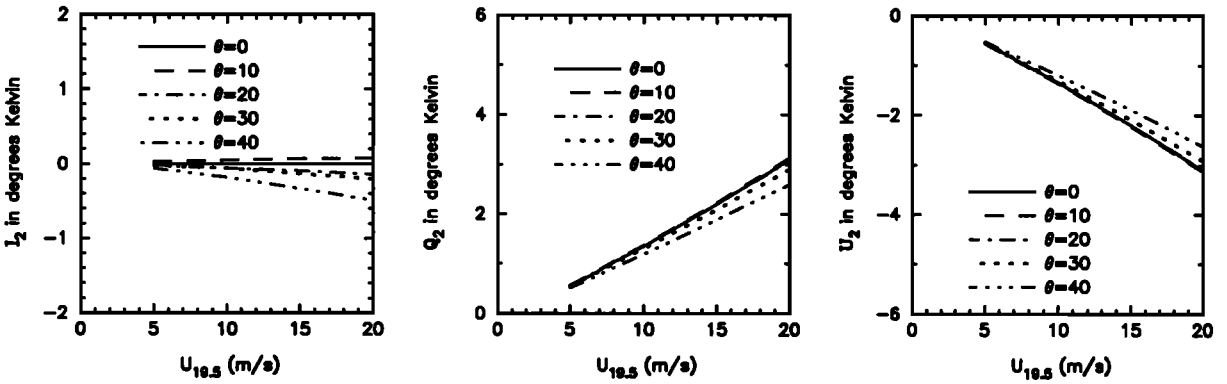

Figure 12. Wind speed dependence at 19.35 GHz. Surface parameters are the same as those of Figure 9. The cutoff wavenumber k_d is 120.

The results presented in Figures 11 and 12 indicate that the theoretical values of Stokes parameters near nadir angles for small-scale sea surfaces can be approximated as:

$$\begin{aligned} I &\simeq a_i + g(U_{19.5}) \\ Q &\simeq Q_0(U_{19.5}) + h(U_{19.5}) \cos 2\phi \\ U &\simeq -h(U_{19.5}) \sin 2\phi \\ V &\simeq 0. \end{aligned} \tag{16}$$

Here g is a monotonic increasing function of the wind speed at 19.5 m ($U_{19.5}$), which is consistent with the aircraft-measured wind speed dependence [*Sasaki et al.*, 1987]. In addition, Q_0 weakly depends on the wind speed, and h is a quasi-linear function of $U_{19.5}$ according to the theoretical results presented in Figure 11. Nevertheless, since the tilting effects of the large-scale surface together with other surface features have not been considered, h is likely to be a more complicated function of wind speed for actual sea surfaces. In addition, since we do not consider any up/downwind surface features, like hydrodynamic modulations, the coefficients of first harmonics are not expected to be zero for real ocean surfaces.

Table 2. Small-Scale Sea Surface Roughness Parameter $k_0\sigma$ Versus Wind Speeds for the Cutoff Wavenumbers k_d = 100 and 120 at f = 19.3 GHz

$U_{19.5}$, m/s	$k_0\sigma$, k_d = 100	$k_0\sigma$, k_d = 120
5	0.18	0.16
10	0.26	0.22
15	0.33	0.29
20	0.39	0.34

The parameter σ is the rms height of small-scale surface.

6. Applications of Polarimetric Radiometry for Ocean Wind Vector Retrieval

This section discusses the application of polarimetric radiometry to ocean wind vector retrieval based on the theoretical form of geophysical model functions derived in previous sections. In particular, we focus on the aspect of wind direction retrieval, since it is well known that spaceborne radiometers already have a demonstrated capability in measuring wind speed. Our emphasis is on how the polarimetric information can enhance the wind direction measurement performance of SSM/I-type instruments.

To start with, it should be noticed that sea surface brightness temperatures are not only affected by wind forcing effects but also affected by several environmental variables, including atmospheric water vapor and cloud water, air and sea surface temperatures, swells, and water salinity. The combining effects of these variables make it a nontrivial problem to invert wind speed and direction using passive brightness temperature measurements.

However, although these environmental variables may affect the azimuth-independent terms I_0 and Q_0, only the wind is expected to have a direct, significant impact on creating the directional fea-

tures on water surfaces. Hence it is anticipated that the amplitudes of azimuth modulations in the brightness temperatures will be dominated by the wind instead of other variables. This allows the wind speed and wind direction inversion problems using passive radiometer measurements to be decoupled to first order.

For wind speed inversion, *Wentz* [1992], using the SSM/I data plus ancillary sea surface temperature map, had already shown that the wind speed and atmospheric water vapor/liquid can be inverted to a sufficient accuracy using multifrequency brightness measurements. On the basis of the wind speed and atmospheric water content information, it is then possible to estimate the magnitudes of Q_0, Q_1, Q_2, U_1, and U_2. Hence it becomes feasible to invert the azimuth angle ϕ using (2) with Q and U measurements.

For example, using the U measurements, which are insensitive to the unpolarized emission from atmospheric water vapor and cloud water, we can determine the wind direction to a few ambiguities. The approach is to relate $\sin \phi$ to $\cos \phi$ using (2),

$$\sin \phi = \frac{U}{U_1 + 2U_2 \cos \phi}, \tag{17}$$

and then substitute the above expression into the trigonometric identity

$$\sin^2 \phi + \cos^2 \phi = 1 \tag{18}$$

The result is a fourth-order polynomial equation for $\cos \phi$, which will yield four or less solutions for ϕ because $\cos \phi$ and $\sin \phi$ have to be real and less than 1. The implication is that U measurements will allow us to infer all possible solutions for ϕ (no more than four).

Besides using U data alone, if it is possible to have an accurate estimate of Q_0 using wind speed and other information, then Q can also be used together with U to estimate wind direction. It can be seen from (2) that Q measurements can provide a quadratic equation for $\cos \phi$, which is an additional constraint for wind direction solution and can reduce the number of possible wind direction solutions to two or even down to one if the magnitude constraint on the cosine and sine functions are applied.

In addition to mathematics arguments, an intuitive way to understand the significance of polarimetric measurements is by comparing the azimuth signature of U with that of I and Q. As evidenced in (2), (4), and (16), it is found that the first two Stokes parameters I and Q have a $\cos 2\phi$ azimuth dependence, while the third Stokes parameter U behaves like $\sin 2\phi$ [$= \cos 2(\phi - 45°)$] in azimuth. This relative phase shift in azimuth makes the U measurements similar to a Q measurement (or T_v and T_h) made at an azimuth angle of 45° with respect to the actual antenna beam pointing direction, meaning that multipolarization measurements made at one azimuth angle are similar to single polarization multiazimuth measurements. The added polarimetric U measurements will therefore effectively improve the geometric configuration for wind direction measurement in the near and far swath portions, where conically scanning, nonpolarimetric radiometers which use fore- and aft-look measurements to estimate the wind direction will not provide good wind direction accuracy because of unfavorable measurement geometry (relative azimuth angle between the fore- and aft-looks close to zero or 180°) in these two areas for wind direction inversion. Hence it is expected that polarimetric measurements will enhance the wind measurement performance of a spaceborne radiometer with SSM/I-like scanning configurations.

Furthermore, if a two-azimuth-look radiometer (an SSM/I type radiometer with a full circle data-taking scan) with U channel is implemented, then the atmospheric water content and other environmental variables effects can be better cancelled out from the Q (or T_v and T_h) measurements by taking the difference of forelook and aftlook data. Using the Q difference and U data will thus ensure good, effective measurement geometry for wind direction inversion (on account of the relative azimuth phase shift between these two Stokes parameters), leading to uniform accuracy for wind direction measurement across all parts of swath.

One final comment is that although we separate the inversion of wind speed and direction in the above discussion for the purpose of illustrating the usefulness of polarimetric data, other inversion schemes, like minimizing the difference between the Stokes parameters measurements with the geophysical model function for simultaneous wind speed and direction estimation, may be more opti-

mal in practice. Thus the optimum scheme, depending on the form of model function and effects of other environmental variables, shall be further investigated.

7. Summary and Discussion

In this paper the theory of polarimetric passive remote sensing of ocean wind is investigated. A second-order SPM is presented to analyze the theoretical form of the geophysical model function of the polarimetric emission from two-dimensional random rough surfaces with an anisotropic directional spectrum. The accuracy of the SPM calculations was quantified by the Monte Carlo simulation technique for the emission from one-dimensional rough surfaces with a power law spectrum. Additionally, we apply the SPM to the small-scale sea surfaces, and theoretical azimuthal variations of Stokes parameters are found to agree reasonably well with aircraft radiometer data [*Dzura et al.*, 1992]. The results of this paper indicate that the passive polarimetry is a promising technique for remote sensing of ocean wind vector and has a potential of providing a uniform wind measurement accuracy across the entire swath.

However, several issues not addressed in this paper need further investigation by either more extended theoretical analyses or measurements to determine the model function of Stokes parameters. In this regard, experiments should be carried out for sea surface emission at a large range of observation angles (θ) from 0° up to 60° or higher, which are important for spaceborne remote sensing applications. In addition, theoretical analysis should be extended to account for the tilting effects of large-scale surfaces and other sea surface features, such as foams, in order to model the up/downwind asymmetry of brightness temperatures observed in SSM/I data. Another issue is the selection of the operational frequency band of the radiometer measurements for ocean wind field applications. In other words, the sensitivity of wind speed and direction versus the microwave frequency should be determined. Finally, the design requirements of a polarimetric radiometer that is capable of measuring at least the first three Stokes parameters with the required accuracy and stability should be studied.

Appendix 1: Polarimetric Bistatic Scattering Coefficients

Let us introduce a polarimetric scattering matrix element $f_{\alpha\beta}(\theta, \phi; \theta_i; \phi_i)$ to describe the scattering from a surface illuminated by a unit amplitude plane wave with the polarization β from the direction (θ_i, ϕ_i). The polarization component α of the scattered field propagating in the direction (θ, ϕ) can be written as

$$E_\alpha = \frac{\exp(ik_0 r)}{r} f_{\alpha\beta}(\theta, \phi; \theta_i, \phi_i),$$

where r is the range from the receiver to the scattering target, and k_0 is the free space wavenumber. Given that, the polarimetric bistatic scattering coefficients can be defined as

$$\gamma_{\alpha\beta\mu\nu}(\theta, \phi; \theta_i, \phi_i) = \frac{4\pi\langle f_{\alpha\beta}(\theta, \phi; \theta_i, \phi_i) f^*_{\mu\nu}(\theta, \phi; \theta_i, \phi_i)\rangle}{A \cos\theta_i},$$

where A is the illuminated area.

Appendix 2: First-Order Scattering Coefficients

The coefficients for the incoherent bistatic scattering coefficients due to the first-order scattered fields are defined as

$$\Gamma_{\alpha\beta\mu\nu}(k_x, k_y, k_{xi}, k_{yi}) = f^{(1)}_{\alpha\beta}(\theta, \phi; \theta_i, \phi_i) f^{(1)*}_{\mu\nu}(\theta, \phi; \theta_i, \phi_i)$$

with

$$f^{(1)}_{hh}(\theta, \phi; \theta_i, \phi_i) = \frac{2k_{zi}(k_1^2 - k_0^2)}{k_z + k_{1z}} \frac{1}{k_{zi} + k_{1zi}} \cdot \left(\frac{k_{xi}}{k_{\rho i}}\frac{k_x}{k_\rho} + \frac{k_{yi}}{k_{\rho i}}\frac{k_y}{k_\rho}\right)$$

$$f^{(1)}_{hv}(\theta, \phi; \theta_i, \phi_i) = \frac{2k_{zi}(k_1^2 - k_0^2)}{k_z + k_{1z}} \frac{k_{1zi}k_0}{k_1^2 k_{zi} + k_0^2 k_{1zi}} \cdot \left(-\frac{k_{yi}}{k_{\rho i}}\frac{k_x}{k_\rho} + \frac{k_{xi}}{k_{\rho i}}\frac{k_y}{k_\rho}\right)$$

$$f_{vh}^{(1)}(\theta, \phi; \theta_i, \phi_i) = \frac{2k_{zi}(k_1^2 - k_0^2)}{k_1^2 k_z + k_0^2 k_{1z}} \frac{k_{1z}k_0}{k_{zi} + k_{1zi}} \cdot \left(-\frac{k_{yi}}{k_{\rho i}} \frac{k_x}{k_\rho} + \frac{k_{xi}}{k_{\rho i}} \frac{k_y}{k_\rho} \right)$$

$$f_{vv}^{(1)}(\theta, \phi; \theta_i, \phi_i) = \frac{2k_{zi}(k_1^2 - k_0^2)}{k_1^2 k_z + k_0^2 k_{1z}} \frac{1}{k_1^2 k_{zi} + k_0^2 k_{1zi}} \cdot \left[k_1^2 k_\rho k_{\rho i} - k_0^2 k_{1z} k_{1zi} \left(\frac{k_{xi}}{k_{\rho i}} \frac{k_x}{k_\rho} + \frac{k_{yi}}{k_{\rho i}} \frac{k_y}{k_\rho} \right) \right],$$

where

$$k_{\rho i} = k_0 \sin \theta_i$$

$$k_{xi} = k_{\rho i} \cos \phi_i$$

$$k_{yi} = k_{\rho i} \sin \phi_i$$

$$k_{zi} = \sqrt{k_0^2 - k_{\rho i}^2}$$

$$k_{1zi} = \sqrt{k_1^2 - k_{\rho i}^2}$$

$$k_\rho = k_0 \sin \theta$$

$$k_x = k_\rho \cos \phi$$

$$k_y = k_\rho \sin \phi$$

$$k_z = \sqrt{k_0^2 - k_\rho^2}$$

$$k_{1z} = \sqrt{k_1^2 - k_\rho^2}$$

and k_0 and k_1 are the electromagnetic wavenumbers of the free space and lower half-space.

Appendix 3: Second-Order Scattering Coefficients

The correction terms of the coherent reflection matrix due to the second-order scattered field are given as follows:

$$f_{hh}^{(2)} = \frac{k_1^2 - k_0^2}{k_{zi} + k_{1zi}} \frac{2k_{zi}}{k_{zi} + k_{1zi}} \left\{ k_{1zi} + \frac{(k_0^2 - k_1^2)}{(k_\rho^2 + k_{1z}k_z)(k_z + k_{1z})} \cdot \left[k_{1z}k_z + k_\rho^2 \left(\frac{k_{xi}}{k_{\rho i}} \frac{k_x}{k_\rho} + \frac{k_{yi}}{k_{\rho i}} \frac{k_y}{k_\rho} \right)^2 \right] \right\}$$

$$f_{vh}^{(2)} = \frac{k_1^2 - k_0^2}{k_{zi} + k_{1zi}} \frac{2k_0 k_{zi}}{k_1^2 k_{zi} + k_0^2 k_{1zi}} \left(\frac{k_{xi}}{k_{\rho i}} \frac{k_y}{k_\rho} - \frac{k_{yi}}{k_{\rho i}} \frac{k_x}{k_\rho} \right) \cdot \left[\frac{k_\rho k_{\rho i} k_1^2}{k_\rho^2 + k_{1z}k_z} + \frac{k_{1zi}k_\rho^2(k_0^2 - k_1^2)}{(k_\rho^2 + k_{1z}k_z)(k_z + k_{1z})} \left(\frac{k_{xi}}{k_{\rho i}} \frac{k_x}{k_\rho} + \frac{k_{yi}}{k_{\rho i}} \frac{k_y}{k_\rho} \right) \right]$$

$$f_{hv}^{(2)} = -f_{vh}^{(2)}$$

$$f_{vv}^{(2)} = \frac{k_0^2 - k_1^2}{k_1^2 k_{zi} + k_0^2 k_{1zi}} \frac{2k_{zi}k_1^2 k_0^2}{k_1^2 k_{zi} + k_0^2 k_{1zi}} \cdot \left\{ \frac{k_{\rho i}^2 k_\rho^2 (k_1^2 - k_0^2)}{k_0^2 (k_\rho^2 + k_{1z}k_z)(k_z + k_{1z})} + k_{1zi} \left[1 - \frac{2k_{\rho i}k_\rho}{k_{1z}k_z + k_\rho^2} \left(\frac{k_{xi}}{k_{\rho i}} \frac{k_x}{k_\rho} + \frac{k_{yi}}{k_{\rho i}} \frac{k_y}{k_\rho} \right) \right] + \frac{k_{1zi}^2 (k_0^2 - k_1^2)}{k_1^2 (k_z + k_{1z})} \cdot \left[1 - \frac{k_\rho^2}{k_{1z}k_z + k_\rho^2} \left(\frac{k_{xi}}{k_{\rho i}} \frac{k_x}{k_\rho} + \frac{k_{yi}}{k_{\rho i}} \frac{k_y}{k_\rho} \right)^2 \right] \right\},$$

where k_{xi}, k_{yi}, $k_{\rho i}$, k_{zi}, k_{1zi}, k_ρ, k_z, and k_{1z} are the same as those defined in Appendix 2.

Appendix 4: Empirical Sea Surface Spectrum

The surface spectrum proposed by *Durden and Vesecky* [1985] for $k > k_j = 2$ is given as

$$W(k, \phi) = \frac{1}{2\pi k} S(k) \Phi(k, \phi),$$

where

$$S(k) = a_0 k^{-3} \left(\frac{bku_*^2}{g_*} \right)^{a \log_{10}(k/k_j)}$$

$$\Phi(k, \phi) = 1 + c(1 - e^{-sk^2}) \cos 2\phi.$$

Here $g_* = g + \gamma k^2$ with $\gamma = 7.25 \times 10^{-5}$, $a = 0.225$, $b = 1.25$, and $g = 9.81$. The value of a_0 represents the absolute magnitude of the spectrum.

The wind speed given at any elevation z can be calculated from u_* by

$$U(z) = \frac{u_*}{0.4} \log \left(\frac{z}{Z_0} \right),$$

where u_* is related to Z_0 by

$$Z_0 = 0.0000684/u_* + 0.00428u_*^2 - 0.000443.$$

The coefficients of the angular part of the spectrum are

$$c = \left(\frac{1-R}{1+R}\right)\frac{2}{(1-D)},$$

where

$$R = \frac{0.003 + 0.00192U(12.5)}{0.00316U(12.5)}$$

$$D = \frac{\int_0^\infty k^2 S(k) e^{-sk^2}\, dk}{\int_0^\infty k^2 S(k)\, dk}.$$

Misprints are found in the equations for Z_0, c, and R in the paper by *Durden and Vesecky* [1985].

Acknowledgments. This work was performed under contract with the National Aeronautics and Space Administration at the Jet Propulsion Laboratory, California Institute of Technology. The authors would like to thank S. Durden and Y. Kim for many valuable discussions and information.

References

Durden, S. P., and J. F. Vesecky, A physical radar cross-section model for a wind-driven sea with swell, *IEEE J. Oceanic Eng., 10*, 445–451, 1985.

Dzura, M. S., V. S. Etkin, A. S. Khrupin, M. N. Pospelov, and M. D. Raev, Radiometers-Polarimeters: Principles of design and applications for sea surface microwave emission polarimetry, paper presented at International Geoscience and Remote Sensing Symposium, Inst. of Electr. and Electron. Eng., Houston, 1992.

Etkin, V. S., et al., Radiohydrophysical Aerospace Research of Ocean, *Rep. IIp-1749*, Acad. of Sci., USSR, Space Res. Inst., Moscow, 1991.

Johnson, J. T., J. A. Kong, R. T. Shin, D. H. Staelin, K. O'Neill, and A. W. Lohanick, Third stokes parameter emission from a periodic water surface, *IEEE Trans. Geosci. Remote Sens., 31*, 1066–1080, 1993.

Johnson, J. T., J. A. Kong, R. T. Shin, S. H. Yueh, S. V. Nghiem, and R. Kwok, Polarimetric thermal emission from rough ocean surfaces, *J. Electromagn. Waves Appl., 8*, 43–59, 1994.

Klein, L. A., and C. T. Swift, An improved model for the dielectric constant of sea water at microwave frequencies, *IEEE Trans. Antennas Propag., 25*, 104–111, 1977.

Nghiem, S. V., M. E. Veysoglu, R. T. Shin, J. A. Kong, K. O'Neill, and A. Lohanick, Polarimetric passive remote sensing of a periodic soil surface: Microwave measurements and analysis, *J. Electromagn. Waves Appl., 5*, 997–1005, 1991.

Peake, W. H., Interaction of electromagnetic waves with some natural surfaces, *IEEE Trans. Antennas Propag., 7*, 8324–8329, 1959.

Sasaki, Y., I. Asanuma, K. Muneyama, G. Naito, and T. Suzuki, The dependence of sea-surface microwave emission on wind speed, frequency, incidence angle, and polarization over the frequency range from 1 to 40 GHz, *IEEE Trans. Geosci. Remote Sens., 25*, 138–146, 1987.

Smith, P. M., The emissivity of sea foam at 19 and 37 GHz, *IEEE Trans. Geosci. Remote Sens., 26*, 541–547, 1988.

Tsang, L., Polarimetric passive remote sensing of random discrete scatterers and rough surfaces, *J. Electromagn. Waves Appl., 5*, 41–57, 1991.

Tsang, L., J. A. Kong, and R. T. Shin, *Theory of Microwave Remote Sensing*, Wiley-Interscience, New York, 1985.

Veysoglu, M. E., S. H. Yueh, R. T. Shin, and J. A. Kong, Polarimetric passive remote sensing of periodic surfaces, *J. Electromagn. Waves Appl., 5*, 267–280, 1991.

Wentz, F. J., Measurement of oceanic wind vector using satellite microwave radiometers, *IEEE Trans. Geosci. Remote Sens., 30*, 960–972, 1992.

Wu, S. T., and A. K. Fung, A noncoherent model for microwave emissions and backscattering from the sea surface, *J. Geophys. Res., 77*, 5917–5929, 1972.

Yueh, S. H., and R. Kwok, Polarimetric passive remote sensing of terrain surfaces, paper presented at International Geoscience and Remote Sensing Symposium, Inst. of Electr. and Electron. Eng., Houston, 1992.

Yueh, S. H., and R. Kwok, Electromagnetic fluctuations for anisotropic media and the generalized Kirchhoff's law, *Radio Sci., 28*, 471–480, 1993.

Yueh, S. H., R. T. Shin, and J. A. Kong, Scattering of electromagnetic waves from a periodic surface with random roughness, *J. Appl. Phys., 64*, 1657–1670, 1988.

Yueh, S. H., S. V. Nghiem, R. Kwok, W. J. Wilson, F. K. Li, J. T. Johnson, and J. A. Kong, Polarimetric thermal emission from periodic water surfaces, *Radio Sci., 29*, 87–96, 1994.

J. A. Kong, Research Laboratory of Electronics, Massachusetts Institute of Technology, 77 Massachusetts Avenue, Cambridge, MA 02139.

R. Kwok, F. K. Li, S. V. Nghiem, W. J. Wilson, and S. H. Yueh, Jet Propulsion Laboratory, California Institute of Technology, 4800 Oak Grove Drive, Pasadena, CA 91109.

(Received May 19, 1993; revised January 4, 1994; accepted January 4, 1994.)